STOCHASTIC MODELLING OF WOVEN COMPOSITES

M. B. Whiteside[1*], S. T. Pinho[1]

[1]*Aeronautics Department, Imperial College London, South Kensington Campus, London, SW7 2AZ*
**martin.whiteside@imperial.ac.uk*

Keywords: Uncertainty Analysis, 2D Woven Composite, Reduced Unit Cell, Monte Carlo Simulation

Abstract

A reduced unit cell (rUC) structural/mechanical model of a 5-Harness satin weave is constructed and analysed deterministically in uniaxial and biaxial loading conditions. An algorithm is developed and implemented to fully automate the rUC construction such that stochastic variations of the crimp angle can be evaluated. Monte Carlo Simulation is employed to propagate the effect of the crimp angle through the deterministic model and the probabilistic response compared with data obtained experimentally. It is observed how simulated variability compares well in uniaxial compression, but under-predicts observed experimental variability in uniaxial tension. The influence of vertical stacking sequence of plies is also demonstrated through the study of in-phase and out-of-phase periodic boundary conditions in the through thickness direction.

1 Introduction

Orthogonal woven or textile composites consist of individual fibres bundled into two sets of tows (typically ranging from 3000 - 6000 fibres per tow), which are interlaced to form a fabric. The choice of weave type influences the anisotropy of material properties. In contrast to unidirectional (UD) composites, the presence of off-axis tows increases the strength and stiffness when subject to in-plane biaxial loading conditions. The tradeoff, however, is reduced strength and stiffness under uniaxial longitudinal loading due to the interlacings within the weave. This gives rise to crimping of the tows, which can be represented quantitatively by a crimp angle, Θ, Figure 1.

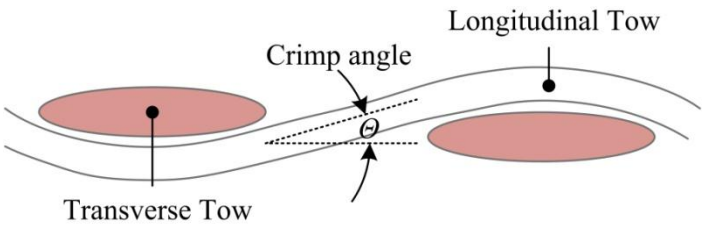

Figure 1. Crimp angle, Θ, definition.

Unlike UD composites, tow interlacing and associated crimp angles of woven composites introduce further complexity to the modelling process [1], the effects of which are exacerbated by ply stacking sequence and tow nesting. These uncertainties and their perceived implications on global material strength properties, leads to the selection of both

conservative design allowables and inflated safety factors when woven composites are employed in primary structural components.

The importance of tow crimp angle on woven composite response has been highlighted within the literature [1], but its effect on material strength variability has yet to be explored. The objective of the work presented within this paper is to develop a parametric Finite Element model of a 5-Harness satin weave (5HS) to simulate the homogenised material stiffness and strength and then to utilise it to investigate the qualitative effects of stochastic variations of the crimp angle, Θ, on the probabilistic response. The simulations are compared and validated with experimental results of Hexcel's carbon fibre epoxy M56/40%/280H5/AS4-3K composite, performed at Imperial College London, of an 8-ply laminate of the same material under uniaxial loading conditions [2]. The model is then extended to construct biaxial stochastic failure envelopes.

2 Methodology

In order to gain an understanding of the underlying failure mechanics, the model is developed on the meso-scale, explicitly modelling tows and matrix. Monte Carlo Simulation is selected as the stochastic analysis methodology, permitting an analysis of the response cloud and detailed analysis of the individual FE model samples and associated failure predictions.

2.1 Finite Element Model

A reduced Unit Cell was defined to represent the 5HS, taking advantage of both translational and rotational symmetries of the weave. Following the framework proposed by Carvalho et al. [3], the traditional UC model, Figure 2a is decomposed into the rUC model, illustrated in Figure 2c.

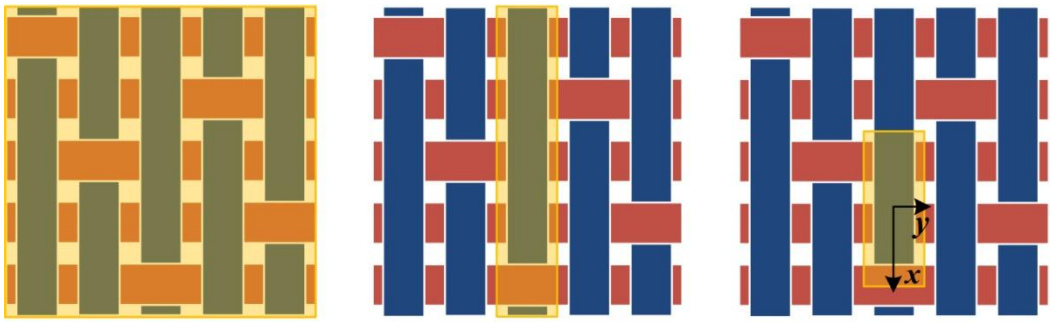

Figure 2: Illustrations of (a) full, (b) translational and (c) reduced Unit Cell (rUC).

In-plane periodic boundary conditions are applied on each face of the rUC to ensure the displacements of the FE model account for the effects of the adjacent rUCs that comprise the global weave structure. In addition, the effect of stacking sequence of plies when combined into a laminate is considered by applying PBCs on the top and bottom surfaces. Three systematic cases are defined illustrated in Figure 3.

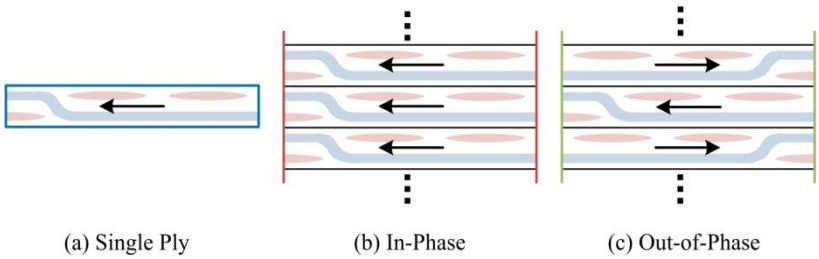

Figure 3: Stacking sequences represented through boundary conditions: (a) Single Ply (Ply), (b) In-Phase (IP), (c) Out-of-Phase (OP).

2.2 Post-processing

Damage initiation in the tows is modelled through use of physically based matrix failure criteria [4]. Because of the woven architecture of the 5HS and the consequent load redistribution to non-failed tows, matrix failure in the tows is not assumed to result in catastrophic failure of the material. Instead, catastrophic failure of the composite is simulated via fibre tensile and fibre kinking modes also derived in [4] , evaluated in the local orientation co-ordinate system of the tow elements.

2.3 Input Characterisation

Where possible, the geometry of the tow is calibrated to measurements obtained experimentally from different studies, however some parameters were estimated within the bounds imposed by the rUC assumption and predefined geometry of the tows. The crimp angle is represented as a Normal distribution with 20° mean and 2° standard deviation. The stiffness and strength properties are selected to coincide with the properties of Hexcel's M56/40%/280H5/AS4-3K composite. Within this analysis the tow is considered to be similar to a UD ply, in the sense that it consists of a number of fibres embedded in a matrix-rich region. Unfortunately experimental characterisation of UD M56/AS4 is not available, and instead Chamis' analytical homogenisation formulae [5] are utilised to derive matrix and tow properties from alternative UD ply and AS4 data provided by Hexcel. The applied material properties are summarised in Table 1.

Parameter	Syntax	Units	Value
Matrix			
Longitudinal modulus	$E_{m,11}$	MPa	4000
In-plane shear modulus	$G_{m,12}$	MPa	1500
Poisson's ratio	$\upsilon_{m,12}$		0.35
Tensile strength	σ_m^+	MPa	60
Compressive strength	σ_m^-	MPa	140
Tow			
Longitudinal modulus	$E_{t,11}$	GPa	180
Transverse modulus	$E_{t,22}$	GPa	11
In-plane shear modulus	$G_{t,12}$	GPa	6.8
In-plane Poisson's ratio	$\upsilon_{t,12}$		0.3
Transverse Poisson's ratio	$\upsilon_{t,23}$		0.4
Longitudinal tensile strength	σ_{tL}^+	MPa	2500
Longitudinal compressive strength	σ_{tL}^-	MPa	1700
Transverse tensile strength	σ_{tT}^+	MPa	80
Transverse compressive strength	σ_{tT}^-	MPa	130
In-plane shear strength	τ_{tT}^+	MPa	115

Table 1. Matrix and tow stiffness and strength parameters

3 Deterministic Results and Discussion

The deterministic model response is evaluated under uniaxial tension and compression with nominal geometric parameters. The maximum stress concentrations and related failure indices are located in the xy-midplane of the rUC and the subsequent stress and failure index diagrams are presented in this profile.

3.1 Uniaxial Tension

The response of the rUC in the Ply, IP and OP configurations under uniaxial tension is presented in Figure 4 and compares them to a series of experiments on 8-ply, carbon fibre epoxy 5HS laminates (M56/40%/280H5/AS4-3K). The stiffness of the IP and OP cases demonstrate excellent agreement to the experimental data at low strain, although fail to capture the apparent strain hardening of the material at higher strain. The stiffness and strength of the Ply case is modelled significantly below that of the IP and OP cases, as should be expected given the lack of through thickness support.

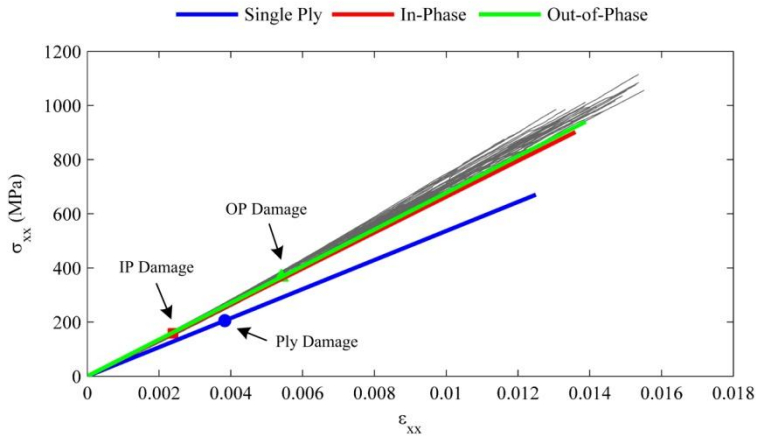

Figure 4: Comparison between experimental and numerically obtained constitutive behavior in uniaxial tension.

In uniaxial tension, the mode that governs failure can be shown to be fibre tensile failure of the tows. Figure 5 shows how the location of this final failure moves from the curvature of the crimp region in the Ply and IP case, to the straight tow region for the OP case.

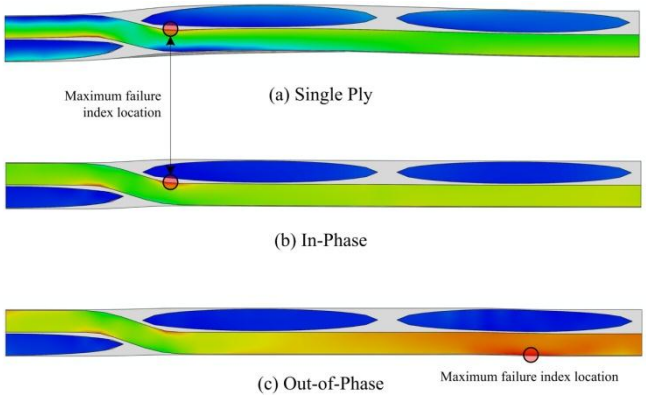

Figure 5: Fibre tensile failure, f_{ft}, distributions along the x-y midplane for uniaxial tension.

3.2 Uniaxial Compression

The model's response to uniaxial compression is illustrated in Figure 6. The Ply model exhibits reduced stiffness in comparison the experimental results, although in this case, both IP and OP models over-predict the experimental stiffness for large strain.

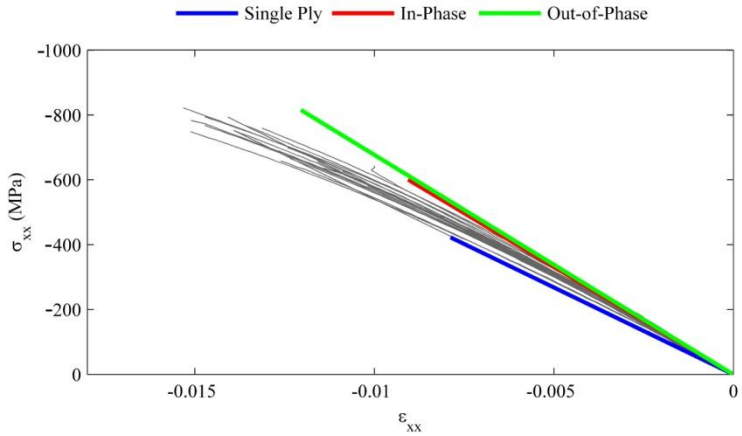

Figure 6: Comparison between experimental and numerically obtained constitutive behavior in uniaxial compression.

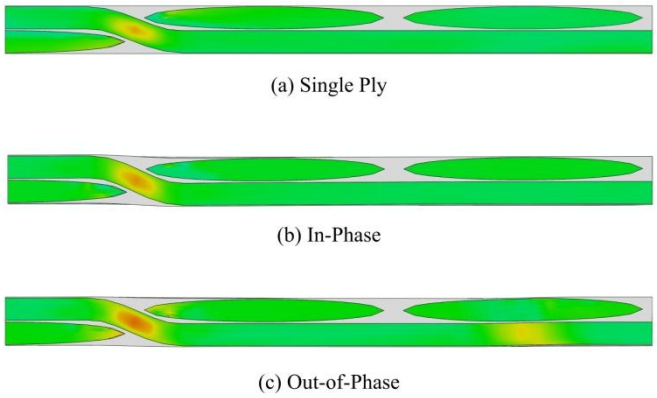

Figure 7: Fibre kinking, f_{kink}, distributions along the xy-midplane for uniaxial compression.

Figure 6 indicates significant disparity between the predicted failure strengths of Ply, IP and OP cases. Under uniaxial compression the dominant failure mechanism is fibre kinking failure of the tows, and from reviewing Figure 7 it is clear that failure is located within the crimp of the tow for each case. Matrix damage initiation is predicted after fibre kinking failure in uniaxial compression for every case.

4 Stochastic Results and Discussion

4.1 Uniaxial Variability

Stochastic results from the MCS of the FE rUC model utilising 100 samples for each loading condition can be compared with those obtained experimentally. Figure 8 illustrates the cumulative density functions of the Ply, IP and OP numerical for uniaxial tension data compared with experimental results. It can be seen again how the average strength simulated by each model under-predicts the average measured strength obtained experimentally. The plot also serves to highlight how the modelled variance resulting from the stochastic variation in crimp angle under predicts the variance observed experimentally.

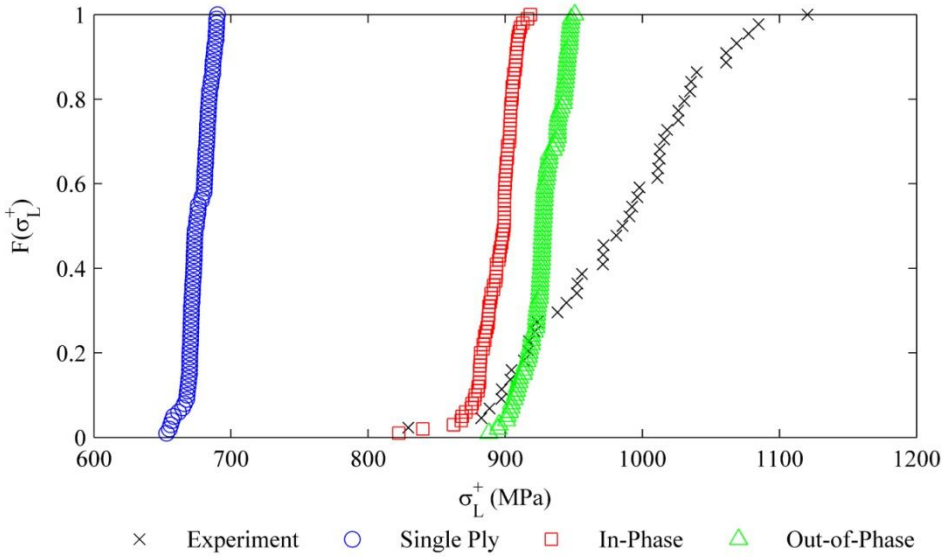

Figure 8: Comparison of Single Ply, In-Phase and Out-of-Phase CDFs with experimental data in tension.

Figure 9 illustrates the comparison of modelled and experimental variability in uniaxial compression and it is immediately apparent that a better match is achieved here. It can be demonstrated that increases in crimp angle results in a considerable reduction in compressive strength and the influence of the crimp angle is concluded to be of primary importance. A quantitative comparison between experimental and numerical results requires size effects to be accounted.

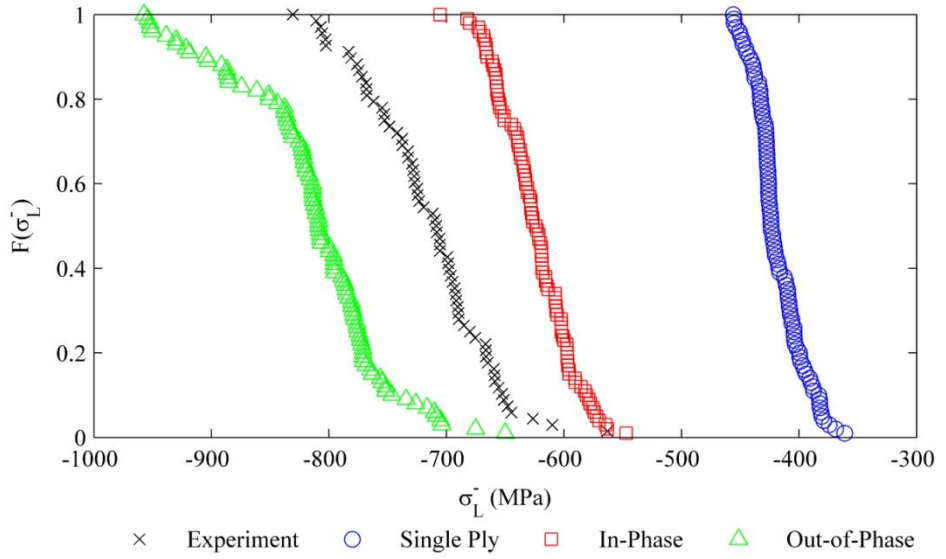

Figure 9: Comparison of Single Ply, In-Phase and Out-of-Phase CDFs with experimental data in compression.

4.2 Stochastic Failure Envelopes

Figure 10 illustrates a stochastic failure envelope detailing biaxial failure probability for the OP case.

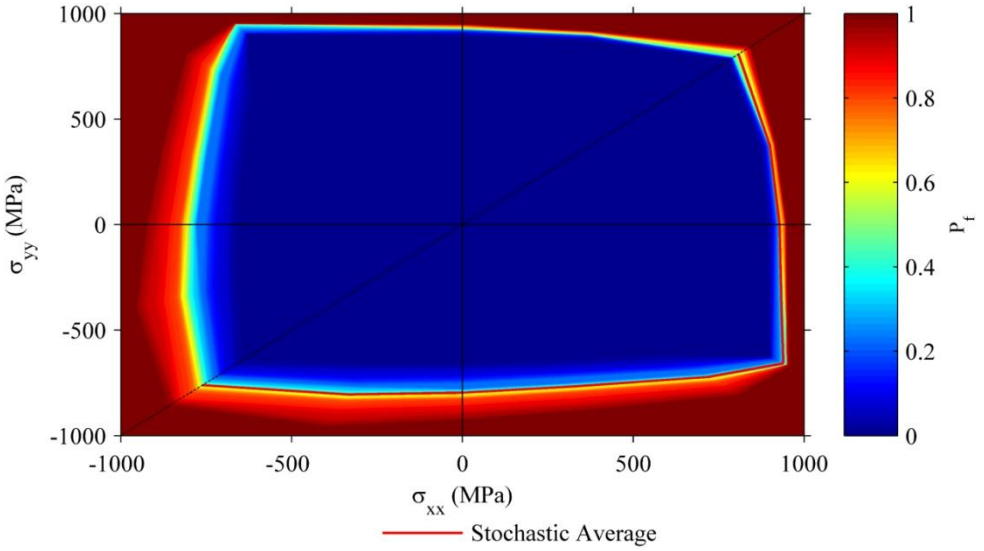

Figure 10: σ_{yy} vs. σ_{xx} Stochastic Failure Envelope for OP model.

Figure 11 presents a comparison of the coefficients of variation, c_v, at various stress ratios, $\alpha = \text{atan}(\sigma_{yy}/\sigma_{xx})$, between each vertical constraint case. It is observed that the introduction of biaxial tensile loading results in no increases in variability in comparison to uniaxial tension. For all loading ratios, it can be concluded that the introduction of through thickness support exacerbates the influence of the crimp angle on the failure response variability. This is particularly relevant to the OP case subject to compression, the variability of which exceeds that simulated by Ply and IP models and experimental results.

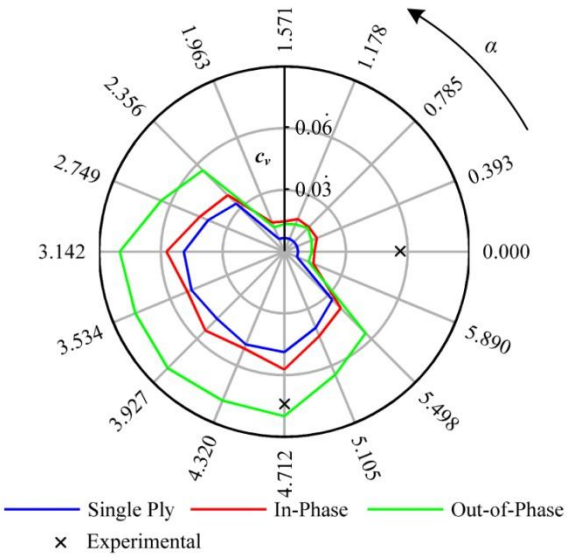

Figure 11: Comparison of coefficient of variation, c_v, between Single Ply, In-Phase and Out-of-Phase models.

5 Conclusions

The simulated deterministic stiffness in uniaxial tension and compression demonstrates encouraging correlation with experimental data. IP and OP cases simulate fibre tensile failure at 894 MPa and 928 MPa in comparison to the experimental average of 980.6 MPa. Failure location can be seen to change from the crimp region in the IP case to the length of the tow in the OP case, providing further evidence of the importance of nesting on failure prediction and modelling. In uniaxial compression, the strength predictions of the IP and OP cases, 624.5 MPa and 813.94 MPa respectively, can be seen to straddle the experimental average of 715.2 MPa, predicting matrix failure in the tow crimp region.

Increases in crimp angle are shown to reduce the strength in both uniaxial tension and compression, the effect being more pronounced in the latter. The simulated variance in uniaxial tension greatly under-predicts that observed in experiment and suggests that other stochastic variables, not considered in this analysis, are important in this domain. Conversely, in uniaxial compression, the variability observed within the simulated results compares favourably with experiment and it is therefore concluded that in compression crimp angle plays a major role in both the mean and observed variability of 2D 5HS woven composite strength.

Stochastic failure envelopes for the Ply, IP and OP models were successfully created. The results graphically illustrate how the variance changes under applied biaxial loading and can be analysed by computing the coefficient of variation of the results at a range of stress ratios. The introduction of through-thickness support in the form of IP and OP boundary conditions results in an increase in simulated variability in comparison to the Ply case. The effect is most apparent in the OP case subjected to compression.

References

[1] N. D. Carvalho, S. Pinho, and P. Robinson, "An experimental study of failure initiation and propagation in 2d woven composites under compression," *Composites Science and Technology*, vol. In Press, Corrected Proof, pp. 1–2, 2011.
[2] C. Niubó Gurgui, "Experimental Stochastic Characterisation of the Failure Process in Woven Composites," 2010.
[3] N. D. Carvalho, S. Pinho, and P. Robinson, "Reducing the domain in the mechanical analysis of periodic structures, with application to woven composites," *Composites Science and Technology*, vol. 71, no. 7, pp. 969 – 979, 2011.
[4] S. Pinho, L. Iannucci, and P. Robinson, "Physically-based failure models and criteria for laminated fibre-reinforced composites with emphasis on fibre kinking: Part i: Development," *Composites Part A: Applied Science and Manufacturing*, vol. 37, no. 1, pp. 63 – 73, 2006.
[5] C. Chamis, "Mechanics of composite materials- past, present and future," *Journal of Composites technology and research*, vol. 11, pp. 3–14, 1989.